Highly stable fluorine-free slippery liquid infused surfaces

Anne-Sophie Vaillard, Manon Saget, Flavie Braud, Marc Lippert, Laurent Keirsbulck, Maude Jimenez, Yannick Coffinier, Vincent Thomy

Highly stable fluorine-free slippery liquid infused surfaces

Anne-Sophie Vaillard , Manon Saget , Flavie Braud , Marc Lippert , Laurent Keirsbulck , Maude Jimenez , Yannick Coffinier , Vincent Thomy

PII: S2468-0230(23)00666-1
DOI: https://doi.org/10.1016/j.surfin.2023.103296
Reference: SURFIN 103296

To appear in: *Surfaces and Interfaces*

Received date: 17 April 2023
Revised date: 12 August 2023
Accepted date: 14 August 2023

Please cite this article as: Anne-Sophie Vaillard , Manon Saget , Flavie Braud , Marc Lippert , Laurent Keirsbulck , Maude Jimenez , Yannick Coffinier , Vincent Thomy , Highly stable fluorine-free slippery liquid infused surfaces, *Surfaces and Interfaces* (2023), doi: https://doi.org/10.1016/j.surfin.2023.103296

Highly stable fluorine-free slippery liquid infused surfaces

Anne-Sophie Vaillard,† Manon Saget ‡,† Flavie Braud,† Marc Lippert, Laurent Keirsbulck,* Maude Jimenez,†,§, Yannick Coffinier, #,† Vincent Thomy,#,†*

† Univ. Lille, CNRS, Centrale Lille, Univ. Polytechnique Hauts-de-France, UMR 8520 - IEMN – Institut d'Electronique de Microélectronique et de Nanotechnologie, F-59000 Lille, France

‡ Univ. Lille, CNRS, INRAE, Centrale Lille, UMR 8207 - UMET – Unité Matériaux et Transformations, Lille, France

§ Institut Universitaire de France, Paris, France

*Université de Valenciennes, Laboratoire LAMIH, UMR CNRS 8201, Le Mont Houy, 59313 Valenciennes, France

[#] **corresponding authors: yannick.coffinier@univ-lille.fr; vincent.thomy@univ-lille.fr**

Abstract

A promising Slippery Liquid Infused Surface (SLIS) has been developed, that is both easy-to-produce and environmentally friendly. Using a double replication method, a 200 µm-thick texturized cross-linked PDMS film was obtained, leading to a grid of micrometric hills and deep wells. A comparison between perfluoropolyether (PFPE) lubricant and silicone oil of different viscosities highlights the advantage of silicone oil, which penetrates the cross-linked PDMS matrix even at high viscosity. Chemical modification with OTS and introduction of secondary structures through plasma etching, increased the surface's shear resistance. As a result, stable sliding properties were maintained, liquid mixtures with low surface tension, after hundreds of cycles of immersion in water and, more originally still after tests under wind blowing exposure

up to 78 m/s. Furthermore, addition of water sprayed during wind blowing exposure allows partial fouling release of the surface.

Keywords: SLIS, polymer molding, lubricant retention, wind tunnel, fouling release

1. Introduction

Surfaces with robust slippery properties can be useful for many kinds of applications such as food industry, submarine surfaces, protection of windscreen in transport or camera lenses. These applications require water barrier and anti-fouling properties in order to mitigate cleaning processes [1–6]. However, the properties of well-known biomimetic repellent surfaces (lotus leaves or butterfly wings) with high roughness or a texturized aspect are severely degraded for low surface tension liquids, as the drop toggles from the metastable Cassie-Baxter to Wenzel state [7–9]. Nevertheless, some biological surfaces, such as *Nepenthes* pitcher plant, disregard the anchoring effect and display slippery properties thanks to its specific structures combining micro and nanoscale roughness retaining wax. The bioinspiration of these remarkable surfaces led to the design of Slippery Liquid Infused Porous Surfaces (SLIPS) by Aizenberg team in 2011 [10].

SLIPS possess a smooth viscous immiscible liquid interface that promotes fluids flow rather than sticking, and prevents fouling. These surfaces provide on-demand lubricant stored in a matrix, enabling them to restore their sliding properties. Even for non-porous surface (called in that case Slippery Liquid Infused Surfaces SLIS), research has been devoted to the influences of morphology and scales of structures, surface chemistry, lubricant nature and viscosity to maintain a stable lubricant layer by promoting long-term self-replenishment [3,11,12].

Structured surfaces can be achieved through multiple methods, which can be divided into two categories: on the one hand, top-down approaches such as laser ablation, plasma treatment, sandblast, phase-separation method, and on the other hand, bottom-up methods like electrospinning, electro-spraying, sacrificial layers, organogel, layer-by-layer deposition, hydrothermal method etc. [1,4,12–21].

Among these techniques, laser ablation has shown significant capacity to produce textured surfaces for a wide range of applications with processing parameters compatible with industrial applications (large number of different materials, large surface, processing time...). It can convey hierarchical structures composed of micro/nano protrusion [22–24]. It has been already reported

that these dual-scale structures promote anti-adhesive and anti-icing characteristics through good lubricant retention by providing strong capillary forces that better retain the lubricant [1,3,12,14,24–27]. For example, Zouaghi *et al.* have developed SLIS, *via* femtosecond laser ablation on stainless steel, followed by fluorosilanization and impregnation with an inert perfluorinated oil. The resulting surfaces present very low CAH of 0.6° and outstandingly mitigate dairy fouling after 90 min of pasteurization test in a pilot-scale equipment [1].

The combination of laser ablation and multiple molding of the patterned surface first developed enables production to be extended by achieving accurate replication of opposing structures [2,22–24,28–30]. Due to its low surface tension and low Young's modulus, cross-linked PDMS appears to be a good candidate to obtain non-wetting surfaces by replication steps [31]. Double replication, using a cross-linked PDMS mold enables the initial textured surface to be quickly and faithfully reproduced, while preserving the fragile texturation from damage [32]. As a result, replication of texturized substrates is cost-efficient and timesaving compared with other texturing techniques for developing high-performance SLIS.

Texturized and/or porous surfaces infused with silicone oil are a promising class of SLIS as they offer environmentally friendly solutions compared to fluorinated based lubricants [5]. Furthermore, silicone oil can both creep up within the cross-linked PDMS matrix and diffuse out to replenish the upper surface when needed. However, the infusion step with silicone oil is a time-consuming due to low penetration process [24]. Authors reported long lasting infusion process achieving steady mass retention after 48h of immersion for low viscosity oil (20 cSt). *A posteriori*, hierarchically textured infused surfaces offer tunable lubricant thickness, displaying more or less immerged surface structures [3,14,24,25,35]. For example, Bandyopadhyay *et al.* have reported double replication molding on rose petal to convey hierarchical structures of 6 µm-high on cross-linked PDMS. By varying the spin-coating speed they were able to adjust the height of a 500 cSt silicone oil layer from 13.2 µm to 1.2 µm. Increasing the lubricant viscosity also makes it possible to increase the lubricant layer thickness, as it provides a higher-shear resistance [12,14,24,27]. Therefore, a viscosity trade-off as to be found between rapid oil penetration or self-replenishment ability, and oil stability on the surface through shear-stress [4,19,33]. For example, Sunny *et al.* have shown that it is possible to improve the endoscope clarity after blood and mucus dipping using a mixed-oil system of low and high viscosity [4].

To assess the durability of the slippery abilities, SLIS need to be characterized under shear stress conditions as close as possible to those of the real application: in terms of water contact and

droplet projection, high air flow interaction and mechanical friction. Ware *et al.* have developed nanostructured wrinkled surfaces that effectively retain silicone oil, after draining by spin-coating and steady shear-stress (60 rpm) for 2 weeks under sea-water [5]. Karkantonis *et al.* submitted texturized polypropylene or polystyrene infused with silicone oil to vortex vibrations, drop dripping cycles, and immersions in food substances and evidenced greater LIS durability with regular sub-micron rather than multi-scale topography [2]. Goodband *et al.* immerged glass functionalized with hydrophobic nanoparticles and infused with silicone oil in aqueous solution. After 12 min of sonication time the hysteresis contact angles increase up to 30° [13]. Many other authors reported various mechanical damages in order to assess the infused surfaces replenishment ability [33,36,37]. Vogel *et al.* described the conservation of highly repellent infused surface based on inverse colloidal monolayers after cleaning with a tissue, scratching with a razor blade or treating with sandpaper [36].

In view of the great application potential of these surfaces, many papers report on their advanced characterization. To this end, we present (i) a texturing technique compatible with a replication and deposition on large surfaces, (ii) the use of liquid impregnation respecting the European safety directives (REACH) and (iii) tests in severe environment conditions (hard water and wind exposures). The texturized surface, easily and faithfully reproducible, through the cross-linked PDMS double replication process, developed in this study, will pave the way for the design of large, long-life out-door SLIS. Through hysteresis angle (CAH) measured after shear driven depletion tests, we demonstrate that chemical and topographic surface modifications offer synergy for sustained oil retention. This promising SLIS can undergo more than hundreds of successive water-dipping cycles, scratching and more than 17 min wind-blowing exposure up to 78 $m.s^{-1}$, before displaying severe degradation of its sliding properties. In addition, we assessed lubricant loss by digital microscopy images through the growing portion of the emerging top of the beveled hills. We evidenced that lubricant level correlates with sliding properties and that hysteresis angles can be predicted by a simple microscopic observation. Finally, spraying water in the wind tunnel showed that the designed SLIS have fouling release behavior.

2. Material and Method

2.1. Samples' preparation

Mold design. The texturized patterns were designed on stainless steel (SS) surfaces by femtosecond laser ablation (300 fs pulse duration and λ=1030 nm). The fluence and frequency of

the pulse were set at respectively 11 J/cm² and 50 kHz. Scanning speeds of 100 mm/s and 0 % transverse area covering corresponding to a spot size of 38 µm were tested. Small SS mold of 2 × 2 cm² was designed. Larger SS mold of 3 × 6 cm² were also designed.

PDMS double replication molding. A commercial PDMS elastomer kit Sylgard™ 184 (Dow Corning, USA) was used to prepare the PDMS base/curing agent mixtures at weight ratio 10:1 and degassed in a planetary centrifugal bubble free mixer (ARV 350, Thinky Mixer) at 2000 rpm under 30 kPa for 1 min. The mixture was poured on the SS mold surface before being placed for 2 hours at 70°C.

After an initial replica molding, the negative samples were coated with a non-sticking layer by plasma RIE of CHF_3 to be used as mold. The 2nd molding consists in spreading 0.45 ml/cm² of degassed PDMS base/curing agent mixtures (10:1) on top of the negative replicate before apply a spin-coating at 500 rpm for 30 s (with 50 rpm/s acceleration). After 1h at 70°C, the block negative mold/positive film was soak in Hexane for 15 min to allow the ultra-thin film to peel off on its own. The films were left in the fume hood for 30 minutes to allow complete evaporation of the hexane.

In order to achieve hierarchical structure, sample O_2CF_4 plasma etching (Plasma Plus 80, Oxford) for 10 min at 300 W, and 30 mTorr with flow rate of 25 sccm and 75 sccm respectively for O_2 and CF_4.

Sticking process. Samples of 2 × 2 cm² and of 3 × 6 cm² were covalently bonded to glass substrate and PMMA substrates respectively. After 1 min O_2 plasma activation, the PMMA plate was immersed for 5 min into a APTMS (3-aminopropyltrimethoxysilane) solution (1% v/v in ethanol) at 80°C to form a self-assembled monolayer (SAM). The plate was then placed for 1h at 80°C to allow the SAM to stabilize [38,39]. After rinsing with isopropanol, the non-texturized side of the PDMS film and the two types of substrates were exposed to corona plasma torch (Corona Treater - Electro-technic Products, Model BD-20V – 230 V, 50-60 Hz, 0.18 A) for 1 min, then put into contact and baked at 90°C for 1h.

Infusion with PFPE-lubricant. A CHF_3-plasma deposition (Plasma Plus 80, Oxford) was achieved for 1 min after 5 min conditioning at plasma power 180 W, flux 50 sccm under 150 mTorr pressure, in order to promote good interactions with the lubricant. It has to be noticed that the CHF_3-plasma coating is also used to form an anti-sticking layer on the mold surfaces that is essential to facilitate the peel off step during the molding process. Perfluorinated lubricants

(Krytox GPL 103 and 105 purchased Dupont de Nemour, USA) (82 cSt and 522 cSt) were used and dropwise deposited on samples top laid flat.

Infusion with silicone oil. After 1 min O_2 plasma activation step (50 sccm 100 W 250 mTorr), samples were coated with Octadecyltrichlorosilane (OTS) layer by chemical vapor deposition for 3h. After rinsing with IPA, samples were immersed in silicone oil bath at 60°C and placed for 1h under dynamic vacuum to expel air contained in the sample then left over one night at atmospheric pressure. Increasing oil temperature reduces viscosity and facilitates penetration into the PDMS film.

After infusion (regardless of the lubricant used), samples were placed vertically to remove excess lubricant gravimetrically before spin-coating (V: 2500 rpm, A: 2500 rpm/s, 30 s, Model: Delta 10, Süss MicroTec, Garching, Germany). Samples were stored in Petri-dishes with closed lids at room temperatures.

2.2. Surface characterizations

The different characterizations were performed on freshly made samples unless specified ageing process applied.

Optical observations. The surfaces were examined optically using digital microscope (X6000, Keyence) before and after lubricant impregnation as well as before and after each depletion test. 2D and 3D image reconstructions were used to qualitatively assess the lubricant level. The lubricant covering rate is estimated from the average surface area covered by the lubricant after binarization over three different 435 µm × 530 µm images (Zoom × 500).

Samples weighing. A microbalance (Mettler Toledo, balance XPR36) was used to weight each sample before impregnation and after the final impregnation step of spin-coating to assess total lubricant retention.

Wettability measurements. Contact Angle (CA) and Contact Angle Hysteresis (CAH) measurements were performed using a drop shape analysis system (DSA100, Krüss, GmbH Germany). CA were measured directly after deposition of a 10 µl drop. Advancing and receding contact angles were measured with 10 µl droplets using the tilting plate method. Tilting table was rotated from 0° to 90° (in steps of 1° per second), and drop deformation and displacement were recorded (50 fps, ten computations per second) while tilting the samples. CAH were calculated from the difference between θ_A and θ_R for four different water-ethanol mixtures (21.7

mN/m < γ < 72.8 mN/m) reported in **Table 1**. Three drops on each sample and two samples with the same laser parameters were measured for statistical uncertainty measurements.

Table 1
Surface tensions of DI water/ethanol mixtures measured using the pendant drop method (averaged over five measurements) [40]

DI water/Ethanol volume ratio	10:0	9:1	3:1	1:1
Mixture surface tension (mN/m)	72.8	52.0	40.0	29.2

2.3. Depletion tests

Water dipping. Samples were dipped in water bath using a dip-coater device, up to 200 cycles up and down were continuously undertaken at 60 mm/min speed with 1 s waiting time at both up and down position.

Wind resistance test. Samples, placed on a 60° inclined plane, were exposed under horizontal 45 $m.s^{-1}$ wind-blowing for 2 min or 15 min. Additional 2 min tests with sputtered water were conducted by progressive release of 10 ml water at the bottom entrance of the fan nozzle. A scheme of the setup is presented in supplementary file **Fig. S1**.

3. Results

PDMS is a non-toxic and transparent polymer commonly used in soft-lithography. Its methyl moieties give it a low surface energy (~ 12 mN/m), rendering a flat cross-linked PDMS hydrophobic (~ 110°). Textured PDMS surfaces of a given roughness display a super-hydrophobic behavior according to the Cassie-Baxter model. However, microstructures increase the adhesive properties of the PDMS substrate (increasing water drop hysteresis) [7,30,31].

The PDMS double replication method from a laser-ablated stainless-steel (SS) mold stands out from the crowd of large, easy and cost-effective structured surfaces. It can be assimilated to existing industrial technics known as hot-embossing or roll-to-roll methods [2]. The study of the texturing of SS molds (laser parameters), carried out upstream, led to a promising surface with a grid-like arrangement. These surfaces feature micrometric pyramidal hills with bevelled tops and a non-uniform height of around 25 µm and a similar width at the base (24.1 ± 1.9 µm). The micro-hills spacing is a few micrometers at the base of the hills and reaches several tens of micrometers at the top. The sub-micrometric roughness, visible on the upper part of the hills,

comes from SS solidification that rapidly cools down after passing laser [22]. At the grid intersection, deep holes with average diameters of 11.6 ± 1.1 µm can be observed. The top view SEM images of the SS mold and both negative and positive PDMS replicates as well as the side view of both replicates are shown in supplementary file **Fig. S2**a, b. In addition, the various surface roughness parameters were assessed on the basis of topographical analysis using digital microscopy (**Fig. S2**c and **Table S1**). The negative replicates present long spikes structures with an estimated maximum total height of 124.9 ±14.0 µm, in agreement with the slice SEM images. The positive replicates, easily obtained through a second replication molding (after plasma coating of the negative replicates), mimic the initial micro-hills and micro-valley structures with deep wells. The positives structures are equivalent to deep close-cells surmounted with small micro-hills of about a quarter of the total thickness of the structured part. Due to deep inner cells, digital microscopy cannot accurately estimate the maximum height of the structured part, but the height of the upper micro-hill is consistent with that determined from SEM images of sample sections.

3.1. Perfluoropolyether as lubricant

A good lubricant acts as a barrier between the working liquid and the PDMS substrate, and imparts non-sticking properties to the surface. First of all, perfluoropolyether (PFPE) based lubricants take pride of place dealing with infused surfaces due to immiscible properties with most common testing liquid [41]. The surface tension between the working liquid and the lubricant must be positive to rule out any chance of miscibility, while a higher value will mitigate the depletion phenomena such as the cloaking or the wetting ridge [25,42]. The choice of the lubricant was also motivated by the remarkable performances of fluorinated synthetic oil (Krytox 103) in extreme environmental conditions such as low pressures (10^{-8} kPa at 20 °C), extremely low or high temperature (-15 to 300 °C), or severe chemical condition (nonreactive and nonflammable). The low vapor pressure of Krytox 103 ensures a low volatility value, leading to a low evaporation rate of 7 % after 22 hours at 121°C [10,42]. Those parameters must be taking into account to promote slippery infused surface with long-term stability.

However, in the case of cross-linked PDMS, chemical treatment with fluorinated compound is required, prior the infusion step, to ensure that the fluorine-based lubricant wets the substrate completely and promotes good interactions. As the lubricant has a low surface tension, it wets the entirely surface perfectly while penetrating the structures easily [3].

Infusion of the texturized surfaces is a crucial step in maximizing the lubricant retention and requires a more appropriate technique [11]. After chemical modification, SLIS were infused for 15 h and successively placed vertically to evacuate the excess of lubricant, then spin-coated to obtain an homogeneous and thin layer independently of the amount of lubricant dropped as displayed in supplementary **Fig. S3**a [5,36,37].

Negative and positives structures treated with PFTS silanization or CHF_3 plasma deposition were compared by measuring the CAH after 10 water-dipping cycles using four different water/ethanol mixtures and reported in supplementary **Fig S2**b, c (along with EDX spectra of both coatings) [43]. Those preliminary results highlighted that positive structures with inner reservoirs combined with CHF_3 coating help the surface to maintain good sliding abilities over a wide range of surface tension liquid.

3.2. Silicone oil-based as lubricant

In addition, in order to comply with REACH regulations, silicone oil (SO) (fluorine free) was used as a lubricant. SO is well-known fouling release coating due to its low surface free energy and low Young's modulus [5,44,45]. The interesting point using cross-linked PDMS as a surface is that SO penetrates within the matrix resulting in its swelling. In this work, the SO infusion process was optimized in terms of processing time and oil saturation by drastically decreasing the thickness of the PDMS films down to 200 µm.

In order to reduce infusion processing time while maximizing oil penetration we have developed a novel technique of Sylgard 184 double replication which results in an ultra-thin PDMS surface as sum up in **Fig. 1**. Soaking the samples in hexane induces swelling of the PDMS samples and produces significant deformation of both replicates. The elongation rate increases as the film thickness decreases. Consequently, the difference in thickness between the two replicas induces a difference in shear stress, leading to films separation. In addition, soaking in hexane reduces the relative mass of a PDMS film by 4.5 ± 0.3 mg due to the removal of residual compounds from the crosslinking reaction.

Fig. 1a shows the top surface, composed of beveled micro-hill. The inner view presented in **Fig. 1**b is obtained while scanning the PDMS film upside down through its transparent bulk and displays wells up to 70 µm deep. **Fig. 1**c illustrates the ultra-thin film with a total thickness of around 200 µm.

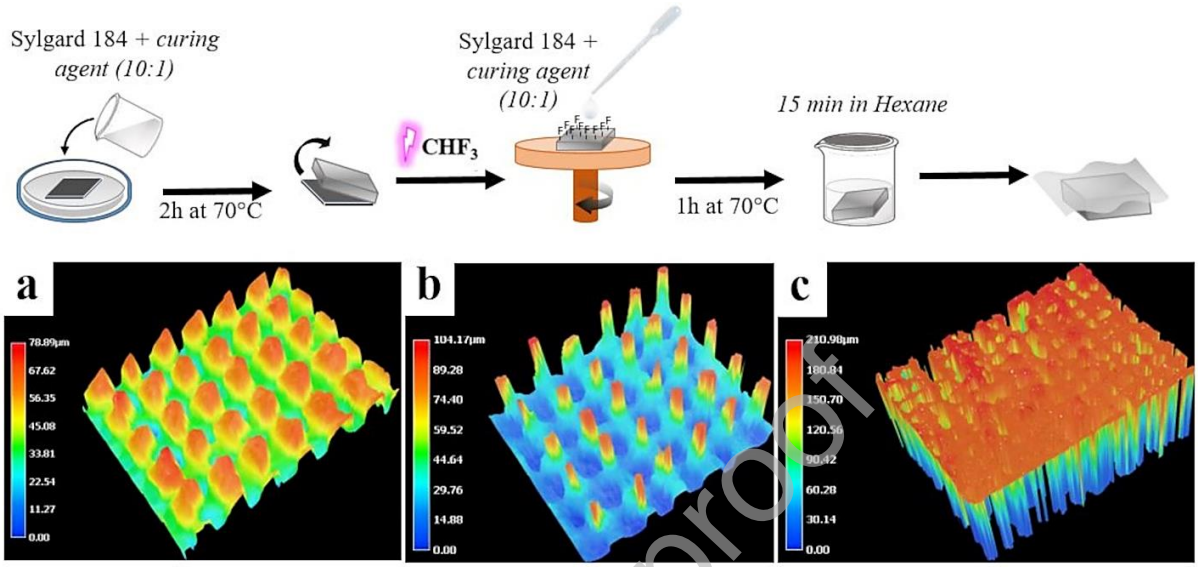

Fig. 1. Schematic diagram of thin films preparation (up). Digital microscopy images of positive replicate (a) top view, (b) inner wells structures of the sample placed upside down and (c) total film thickness.

3.3. Influence of the viscosity for retention of both fluorine and silicone oil based lubricants

Firstly, PFPE based lubricant (K) and silicone oil (SO) with different viscosities, 82 or 522 cSt and 100 or 350 cSt respectively, were investigated in terms of durability through shear stress experiments. Samples K82 or K522 were coated with CHF_3 while no chemical modifications was initially employed for SO100 and SO350 samples due to chemical affinity between PDMS surface and SO. **Table 2** shows the average mass infused of the different lubricant and viscosity weighed after 30 sec of spin-coating at 2500 rpm, as well as the lubricant covering rate assessed from binarized digital microscopy images recorded after spin-coating or water-dipping tests (inset of **Fig. 2**a). After spin-coating at 2500 rpm all SLIS designed present heterogeneous surface with different portion of emergent cross-linked PDMS structures [24]. For more viscous PFPE-lubricant, a higher shear-resistance is reached. It improves the lubricant retention by 34 % and doubles the lubricant covering rate (depending on the hills geometry). In the case of silicone oil, seepage into the film bulk is easier for lower viscosity oil. Lowering the viscosity by a factor of 3.5 increases oil retention by up to 30 %. However, the low-viscosity oil will be slightly less present on the surface as lubricant covering rate is slightly lower. As a result, the two high-

viscosity oils better wrap the surface structures after spin-coating at 2500 rpm, and still cover about 85 % of the surface.

Table 2
Average lubricant mass infused and lubricant covering rate of K82, K522, SO100 and SO350, estimated from digital microscopy images recorded after spin-coating (30 sec at 2500 rpm), and after 30 and 50 cycles of water-dipping

Lubricant	Δm (mg/cm²)	Lubricant covering rate (%)		
		2500 rpm	30 water-dipping	50 water-dipping
K82	5.67 ± 0.8	46.0 ± 2.3	24.3 ± 3.6	22.3 ± 1.1
K522	7.63 ± 0.2	86.5 ± 2.9	56.7 ± 2.7	21.6 ± 2.1
SO100	14.7 ± 1.8	75.3 ± 2.4	33.4 ± 1.7	N/A
SO350	11.3 ± 0.7	85.2 ± 1.8	58.6 ± 4.6	23.3 ± 1.7

Fig. 2a represents the mean contact angles (CA) of the different SLIS as a function of the working liquid surface tension γ_l. Higher CA were recorded on fluorine-SLIS than on silicone-SLIS as reported in the literature [46]. Indeed, after spin-coating, SLIS are widely covered by the lubricant and CA follow the Young's law $\cos(CA) = (\gamma_o - \gamma_{ol})/\gamma_l$ (γ_o and γ_{ol} are respectively the oil surface tension at the air and working liquid interface). Neither the difference of lubricant viscosity nor the lubricant nature affects significantly the oil surface tension γ_o with 17 mN/m and 18 mN/m for respectively K82 and K522 and 21 mN/m for silicone oil [11,47]. However, γ_{ol} is higher for the PFPE lubricant than for silicone oil. Then, the difference $\gamma_o - \gamma_{ol}$ is negative, giving a CA greater than 90° for the entire γ_l range. Nevertheless, a sign change occurs for SO-infused surface resulting in CA smaller than 90° for liquids with low surface tension. The difference of CA between fluorine based and silicone based SLIS grows while decreasing the working liquid surface tension (from about ten to twenty degrees at lower γ_l).

The SLIS have been submitted to successive water immersion resulting in loss of lubricant and progressive exposure of the patterned substrate to the tested drop. This infused surface state has been reported as hemi-wicking [48,49]. When decreasing the lubricant level, the growing

portions of cross-linked PDMS will induce two phenomenon that compete and affect CA. Firstly, the surface turns from rather flat state to a texturized one, and the apparent contact angle must be taken into account [7,25,49]. Consequently, a CA threshold, which depends on the projected solid area, will determine the apparent CA. For CA lower than the threshold, the drop is in the Wenzel state, decreasing the apparent CA. This is the case for liquids with low surface tension, that wet the structures, increasing the drop contact line. For CA above the threshold, the drop lie on air gaps trapped within the secondary structures and the apparent CA rise. It is worth mentioning that, as micro-hills are pyramid-shaped, the projected area of the surface increases, and drastically emphases the apparent CA as lubricant level decreases (micro-hill are wider and their spacing is reduced). Moreover, due to growing fraction of emerged structures the Cassie's law includes a solid contribution part $\cos(CA) = \sigma_o(\gamma_o - \gamma_{ol})/\gamma_l + \sigma_s(\gamma_s - \gamma_{sl})/\gamma_l$ where σ_o and σ_s are respectively the portions of oil and of emergent solid. In the case of fluorinated SLIS, the solid interfacial tension, γ_s, is lower because cross-linked PDMS has been coated with CHF_3 prior the infusion. Therefore, the difference $\gamma_s - \gamma_{sl} < \gamma_o - \gamma_{ol} < 0$ for the whole γ_l range, inducing an increasing CA when σ_l rises.

Successive Water-Dipping (WD), up to 30 cycles, have no significant effects on CA values despite the decrease in lubricant level. This result may indicate that a thin lubricant layer is still wrapping the emergent structures and that solid PDMS is not in contact with the working liquid. At low liquid surface tension, CA recorded on silicone infused surfaces undergo a weak decrease due to a slight increase of the projected surface area because surfaces are less smooth. However, after 20 additional immersion cycles, the emergent solid contribution is no longer negligible. All SLIS exhibit higher CA with high liquid surface tension, whereas, for low liquid surface tension, CA recorded on fluorinated SLIS increase contrary to silicone SLIS.

A wetting ridge is formed around the drop in order to balance the different interfacial tensions involved. It can either accelerate the lubricant depletion as the drop passes through or accelerate it sliding speed. It is worth noting that according to the positive spreading parameter defined as $S_{ol} = \gamma_l - \gamma_o - \gamma_{ol}$, both fluorine based lubricant and silicone oil will cloak the water drop (stronger cloaking for silicone oil) but it is no longer the case when decreasing the surface tension [46]. However as reported in the literature, reducing the lubricant thickness covering the surface decreases the wetting ridge effect [48].

Contact angles hysteresis (CAH) expressed drop mobility that is strongly dependent on the fraction of emergent solid structures due to adhesive properties of textured cross-linked PDMS. **Fig. 2**b displays CAH as a function of the testing liquid surface tension recorded on those surfaces after spin-coating at 2500 rpm and immersion in water for 30 and then 20 additional cycles (50 WD in total). Colorized digital microscopy images of K522 and SO350, presented in inset of **Fig. 2**a, allow for controlling the lubricant levels. Due to pyramid-shaped micro-hills, the lowering of the lubricant level can be followed by top view microscopy images displaying growing portions of cross-linked PDMS. Despite the significant difference of lubricant covering rate recorded after spin-coating, very low hysteresis values are measured, regardless the viscosity nor the lubricant chemical nature. This result confirms the presence of a thin lubricant layer wrapping the emergent structures that allow drops to keep sliding despite the emergence of the PDMS substrate. After 30 successive WD cycles, the lubricant covering rates of K82 and SO100 samples drop to 47 % and 55 % respectively, and hysteresis angles begin to increase, particularly for liquids with lower surface tensions. For a given amount of emergent solid surface, the contact line pinning is higher for low γ_l, due to lower CA. Therefore, the testing liquid is more flatten over the surface and the hysteresis angles is more impacted. The drop moves from a smooth to a rougher surface, more heterogeneous, where the drop impales itself due to highly adhesive properties of the patterned substrate.

Both higher viscosity lubricants exhibit similar level of lubricant covering rates, in full agreement with the CAH values of both surfaces that remain below 10° excepted at the lowest surface tension ($\gamma_l = 29.2$ mN/m). After a total of 50 WD cycles, all lubricant covering rates are similar and very low (below the detection limit for SO100) while hysteresis values are drastically different. For PFPE samples, CAH recorded for K522 are around 25° with a slight increase at very low surface tension, while values recorded for K82 reach 45° and drop pinning was observed at very low surface tension. The water droplet hysteresis measured on SO350 is above 20° and drop pinning was observed for all water-ethanol mixtures (due to increased contact line). SO100 samples showed drop impalement regardless of surface tension. For non-sliding surfaces (up to 90° tilting), no CA was measured and values are not displayed in **Fig. 2**a. **Fig. 2**c shows hysteresis angles recorded after 2 min exposure in wind tunnel at 45 $m.s^{-1}$ and 78 $m.s^{-1}$. Increasing blowing speed induces an increase in hysteresis angles, particularly for both low viscosity lubricant. The slipperiness of K522 and SO350 samples does not seem to be affected by 2 min at 78 $m.s^{-1}$. Although there was no significant difference in hysteresis recorded

after 30 WD cycles on SO100 and SO350 samples, the wind tunnel drastically damaged slipperiness of SO100-impregnated samples compared to SO350-impregnated samples.

As observed in **Fig. 2**b in the case of water immersion cycles, after wind-tunnel experiments at different speed, **Fig. S9**a displays that CA increase for liquids with high surface tension and go down otherwise. This results from the appearance of an increasing portion of cross-linked PDMS as the lubricant disappears. However, this phenomenon remains limited for high viscosity lubricants.

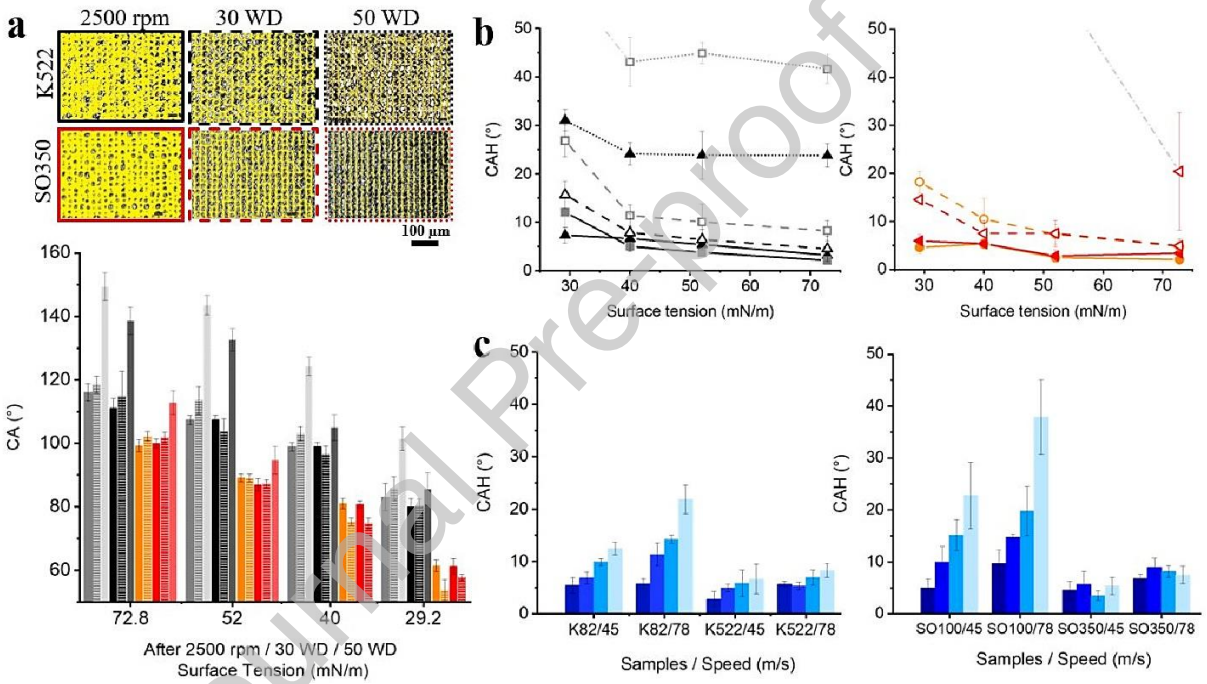

Fig. 2. (a) Contact Angles and (b) Contact Angles Hysteresis as a function of surface tension measured after 2500 rpm spin-coating (full line), 30 cycles of water-dipping (dash) and 50 cycles (dots), on K82 (grey) and K522 (black) samples and on SO100 (orange) and SO350 (red) samples. Inset are the corresponding digital microscopy images. Lighter dash and dot line represent drop pinning. (c) Contact Angles Hysteresis as a function of surface tension after 2 min in wind-tunnel at 45 $m.s^{-1}$ and 78 $m.s^{-1}$ on K82 and K522 samples (left) and on SO100 and SO350 samples (right). The decrease of surface tension corresponds to fading blue histogram bars.

While high viscosity lubricants reduce the sliding speed of drops due to higher friction, the shear resistance of such lubricant is more favorable for the design of durable out-door SLIS [21]. It appears that high viscosity SO is a promising lubricant for cross-linked PDMS based SLIS that

would require chemical modification to improve long-term shear strength and reach PFPE-infused surface performances.

3.4. Influence of additional structuration and chemical treatment on silicone oil retention

In the second part, we investigated ways to improve the durability of SO350 samples through chemical modification and/or nanoscale physical etching performed prior the infusion step.

First of all, chemical modification with octadecyltrichlorosilane (OTS) layer (by CVD) was tested to improve SO spreading and to favor attractive interactions with the lubricant [15,25]. OTS is commonly used as a surface treatment for SO to fully wet the surface (CA of SO measured on cross-linked PDMS goes from 26° to 0° after OTS grafting); leading to a thin oil layer wrapping the exposed texture tops of the surface [15,25].

To create nanoscale roughness on PDMS substrate and induce hierarchical structures (micro-hills and nano-roughness), etching combining oxygen and tetrafluorocarbone (CF_4) gas has already been reported [50,51]. The authors report that an O_2/CF_4 flux ratio of 1:3 offers the highest etch rate, at 20 µm/h (at 270 W and 50 mTorr) [50]. It is worth mentioning that certain quantities of fluorinated compounds resulting from the etching process were detected by EDX (Supplementary **Fig. S4**). However, these traces of fluorine are stable and do not come into contact with the testing liquid due to the presence of an OTS monolayer and/or a lubricant layer. OTS-SO350 and O_2CF_4-SO350 samples were characterized as well as the combination of both technique starting with the etching and named O_2CF_4-OTS-SO350 samples.

Hysteresis measurements were recorded and the corresponding level of lubricant assessed after different numbers of WD cycles to follow the lubricant loss, as display in **Fig. 3**. After being freshly infused and spin-coated at 2500 rpm, the lubricant covers more than 80% of the surface (some visible emergent micro-hills). At this lubricant level, the hysteresis angles of all samples remain low (less than 7°) as display in supplementary **Fig. S4**. One can notice the curves inflection at 52 mN/m with a slight decrease the hysteresis value recorded for the whole sample set. This results from a sign change of the spreading coefficient $S_{os(w)}$ beneath the drop when decreasing the testing liquid surface tension [25,52]. In addition, water-ethanol mixture will tend to a non-clocking behavior on SO infused surface that is favorable to limit the lubricant depletion [41]. After 30 cycles of water immersion, CAH remain low and steady (CAH curve inflection at

52.0 mN/m is no longer recorded), except a slight increase at the lowest surface tension for SO350 and O_2CF_4-SO350 samples. No significant difference between the CAH and the corresponding Sliding Angle (SA) have been recorded, as presented in **Fig. S5**b**.** Oil covering rate recorded on O_2CF_4-SO350 samples is the lowest of the whole sample set at that point. While keeping up immersion cycles, hysteresis values are progressively shifted toward higher values. After additional 20 cycles, the slipperiness of samples with surface modification is maintained contrary to SO350 samples. The SA values follow the same evolution as the CAH values, as it can be seen in **Fig. S5**c. CAH and SA values recorded on O_2CF_4-OTS-SO350 SLIS after 50 WD are similar to those recorded on K522 SLIS after spin-coating (cf. **Fig. S5**d). The values measured on O_2CF_4-SO350 surfaces look like those measured on K522 after 30 WD. Supplementary **Fig. S6** shows the comparison between OTS-SO350 and CHF_3-K522 after 50 WD, highlighting the strength of SO infused samples that maintain lower hysteresis values even at lower viscosity. From **Fig. 3**, one can notice that, OTS-SO350 samples are more affected by those additional stress exposures (50 and 70 cycles in total) than O_2CF_4-SO350 ones, in terms of increased hysteresis and reduced lubricant levels. The acceleration of the lubricant loss for OTS samples compared to O_2CF_4 samples, beyond 30 cycles of water immersion, can be seen in **Fig. S7** with a faster increase of the CAH values while increasing the number of immerging cycles. This behavior can also be observed as curve inversion on **Fig. S8** showing the evolution of the lubricant covering rate as a function of WD number. Finally, samples O_2CF_4-OTS-SO350 are able to maintain a hysteresis angle below 10° for surface tension greater than 40 mN/m, after 70 cycles of water-dipping. The steering coefficient of O_2CF_4-OTS-SO350 lubricant covering rate is lower than for the other samples, as presented in **Fig. S8**. For comparison with porous polymeric matrix infused with fluorinated lubricant, Kazaryan *et al.* report conservation of the sliding properties until 10 immersion cycles that gradually disappear for hexadecane working liquid after prolonged soaking up to 40 cycles while using water as working liquid, wetting properties vanish rapidly due to polar attractive interactions [20]. According to the combination of CAH measurements and digital microscopy images, OTS and O_2CF_4 hamper the lubricant loss. These results highlight a synergy between OTS chemical coating and nano-roughness induced by O_2CF_4 etching in order to impede lubricant depletion. While lubricant occupies most of the surface, the OTS plays an important role in preserving the lubricant. However, when lubricant-covering rate is too low, secondary structures prevail and maintain a thin layer of oil on the emerged micro-hills, preventing drop pinning from occurring to soon. Despite the large number

of emerging micro-hills, a thin layer of lubricant filling the roughness, held in place by intermolecular forces, ensures continuous slippery behavior [53].

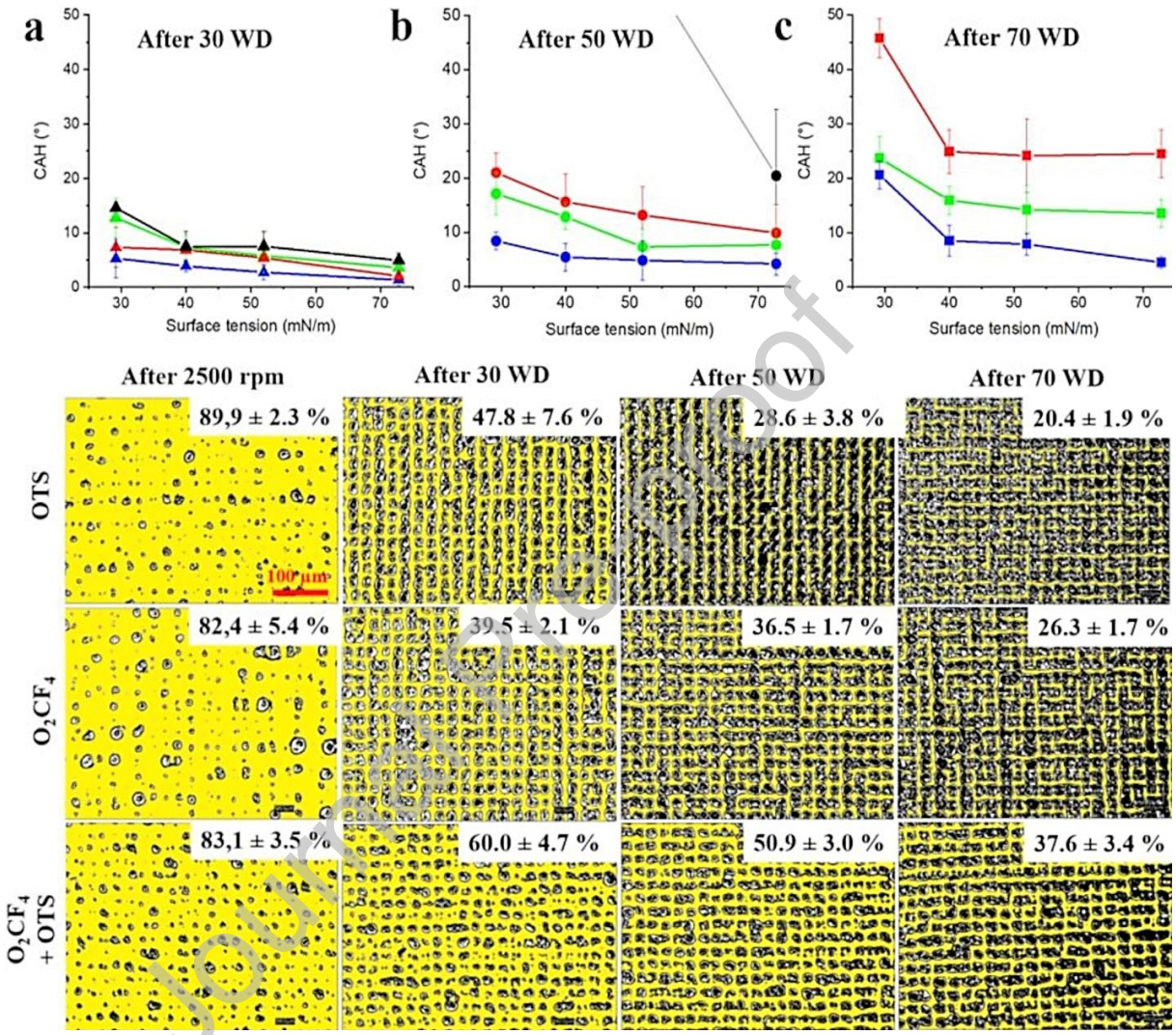

Fig. 3. Contact Angles Hysteresis as a function of surface tension after (a) 30, (b) 50 and (c) 70 cycles of water-dipping for SO350 (black), OTS-SO350 (red), O_2CF_4-SO350 (green) and O_2CF_4-OTS-SO350 (blue) samples. Digital microscopy images and oil covering rate for modified sample after corresponding number of water dipping.

The CA measured on the aforementioned modified SLIS after spin-coating at 2500 rpm and after 30 WD cycles are displayed in **Fig. S9**b. After-spin-coating, CA are the same as for unmodified

SO350 samples, because the infused surface forms almost a flat and uniform interface. After 30 WD, all modified SO350 samples keep a sufficient lubricant level with a thin layer covering the emergent structures then the liquid is only in contact with the lubricant (low CAH). Therefore, CA of high liquid surface tension remains constant while CA decrease at low γ_l due to bigger contact lines that decrease the apparent contact angle. One can notice that CA follows the same trend as for unmodified SO350 samples soaked for 30 cycles due to similar lubricant level covering rate (from 60 % to 50 %). The CA values recorded on O_2CF_4-SO350 surfaces are lower because the lubricant level is lower (47%). Measured CA after 50 and 70 WD cycles, are shown on **Fig. 4** and compared with initial ones (after spin-coating). After 50 WD, CA of O_2CF_4-OTS-SO350 samples keep following the same behavior (constant at high γ_l and decreasing at low γ_l), contrary to OTS-SO350 and to O_2CF_4-SO350 samples recording higher CA at high γ_l. Indeed, lubricant levels of the last samples mentioned (< 40 %) are no longer sufficient to cover the entire emerged structures and interfacial tension of modified cross-linked PDMS is involved. OTS modified surfaces possess a lower interfacial tension γ_s than raw cross-linked PDMS. Interfacial tension of O_2CF_4 is also slightly reduced due to residual fluorine compounds (cf. EDX spectra **Fig. S4**a). Thus, CA do not follow the same trend as for SO100 samples after 30 soaked despite of similar lubricant level (~ 30 %). The difference $\gamma_s - \gamma_{sl}$, from the solid contribution of the Cassie's law, is smaller than for unmodified cross-linked PDMS, then, the increase in CA is greater when the liquid surface tension is high and, at low γ_l, the reduction of the apparent

contact angle is slightly balanced. After 70 WD cycles, the lubricant level of O_2CF_4-SO350 surfaces is similar to OTS-SO350 surfaces after only 50 cycles. Then, it is not surprising to record the same CA measured earlier. For OTS samples, that display the lowest lubricant level, CA jump up to 128° due to air pockets trapped in the nano-roughness, contrary to O_2CF_4 SLIS retaining a small amount of lubricant.

3.5. Impregnation stability tests under severe stress

Depletion tests carried out on O_2CF_4-OTS-SO350 were extended: scratching with a tweezer, water-dipping up to 200 cycles, and 17 min exposure to wind blowing up to 78 m/s with sprayed water.

The replenishment abilities of O_2CF_4-OTS-SO350 samples (after undergoing 70 water-dipping cycles), were observed by digital microscopy after scratching the sample surfaces with a tweezer. **Fig. 5.** displays the corresponding images recorded at different elapsed times. The progressive disappearance of the trace left by the tweezer passing evinces a fast supplying of lubricant within 30 sec. The corresponding self-replenishment video is available in supplementary file. This quick replenishment was made possible by the combination of surficial oil tank, highly deformable elastomeric structures and grid-like channels. Liu *et al.* observed replenishment at a similar speed after knife scratch and evidenced self-healing abilities for interconnected microchannels covered with cross-linked nano-sheets. They showed that several knife scratch along a droplet

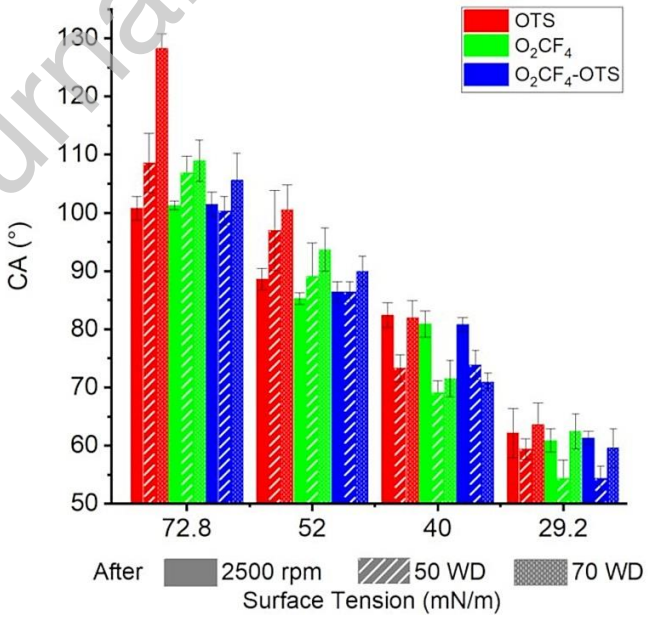

Fig. 4. Contact Angles at different surface tension measured after spin-coating at 2500 rpm, 50 (stripes) and 70 water-dipping cycles on OTS-SO350, O_2CF_4-SO350 and O_2CF_4-OTS-SO350 samples.

pathway did not prevent it from sliding [54]. The slippery property of SLIPS based on polyamide texturized by femtosecond laser by Yong *et al*. could also be quickly self-repaired after multiple knife damage due to silicone oil that spontaneously reinfuses physical voids [55].

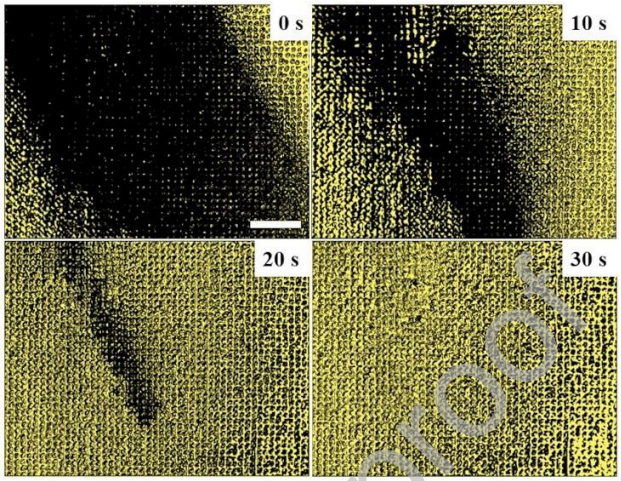

Fig. 5. Digital microscopy images of O_2CF_4-OTS-SO350 scratched (white part) after 70 water-dipping cycles. Scale bars represents 200 µm.

To assess the limits of O_2CF_4-OTS-SO350 samples to water immersion, we increased the number of WD cycles. **Fig. 6**a shows the hysteresis recorded on O_2CF_4-OTS-SO350 samples as a function of the number of WD cycles. The decreasing shades of blue illustrate the increase in ethanol content of the testing liquid, indicating a surface tension sweep from 72.8 to 29.2 mN/m. We recorded severe degradation of the sliding behavior after 100 water-dipping cycles, however, droplet pinning at the lowest surface tension only occurs after 200 WD cycles and large hysteresis angles have been recorded for other surface tension values. When the lubricant level is too low (200 cycles of water immersion), SLIS behave like low energy textured surface as on can see on **Fig S9**c. At high liquid surface tension, they display high CA (up to 130°) due to air gaps trapped beneath the drop in the secondary roughness, while drops of low surface tension are impaled and do not slide or roll on the surface. However, the small base radius of a water drop (small contact line) that led the drag force to overcome the adhesion force is no longer valid when considering low CA values recorded at 40 mN/m, whereas the CAH are no so far apart. The oil covering rate drops at 25.2 ± 1.3 % and 15.6 ± 1.5 % after respectively 100 and 200 cycles of water immersion. Those low values highlight the presence of a thin oil layer wrapping

the micro-hills tops and allowing the sliding behavior to be maintained even after severe lubricant impoverishment.

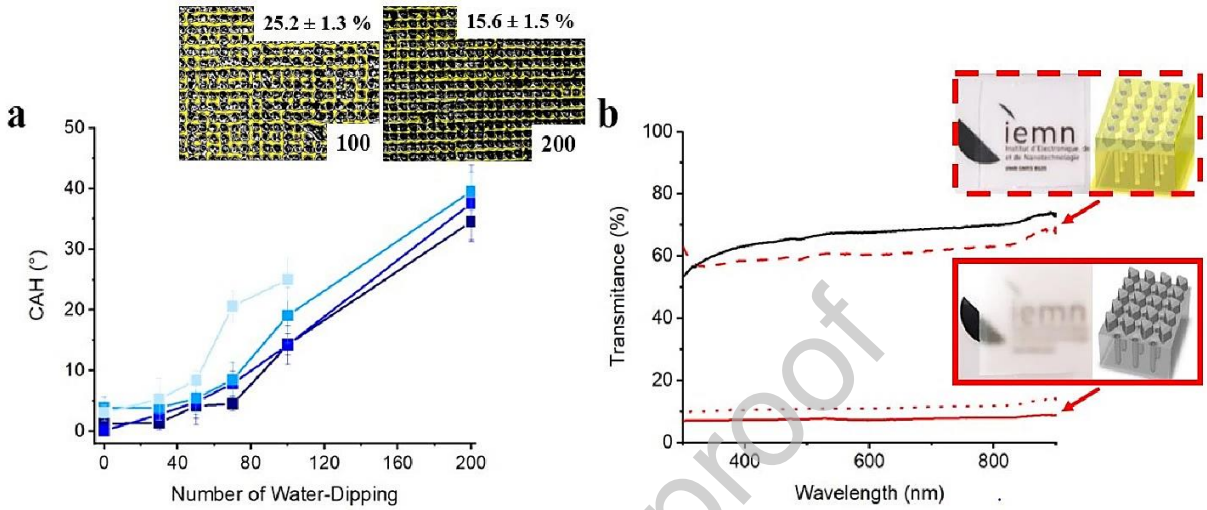

Fig. 6. (a) Contact Angles Hysteresis of O_2CF_4-OTS-SO350 samples as a function of number of water-dipping cycles. The decrease of surface tension corresponds to fading blue lines. Inset are digital microscopy images corresponding to lubricant covering rates after 100 and 200 cycles. (b) Transmittance of 5 mm-thick PDMS (black line) and ultra-thin texturized film (full red line), O_2CF_4-OTS-SO350 (dash line) and O_2CF_4-OTS-SO350 after 200 water-dipping cycles (dots line). Inset are samples (2 × 2 cm²) photography and surface schemes corresponding to dash and dot curves.

Another way to characterize the retention properties of our surfaces is to measure their optical transmission properties in the visible range. Thus, **Fig. 6**b illustrates the transmittance recorded at different step of the elaboration and characterization. Thick and raw PDMS surface has an average transmittance of 68 % that can reach 80 % when decreasing it thickness until hundreds of microns. However, for 200 µm-thick films obtained by double replication molding incorporating micrometer-sized elements, the transmittance drops to 8 %. Transparency recovery is observed after oil infusion process (60 %). However, after 200 WD cycles, the recorded transmittance drops at 10 %. Indeed, samples subjected to harsh test conditions suffer from drastic oil loss, resulting in a significant reduction in transparency, due to exposed micro-hill tops.

Fig. 7a shows the hysteresis values recorded on larger samples (3 × 6 cm²) that experienced high speed wind up to 78 m/s. After 2 min exposure, O_2CF_4-OTS-SO350, hysteresis remained lower than 10°, but a small increase has been recorded for water-ethanol mixtures. By sputtering 10 ml of water, during the same exposure time, the hysteresis values at intermediate surface tension are slightly reduced. Contrary to "dry" exposure, CAH are similar for surface tension ranking from 72.8 to 40.0 mN/m. This may indicate that SLIS possess fouling release properties, allowing elimination of dust particles that hinder drop sliding and disturb the hysteresis measurements. It indicates that a sufficient lubricant amount on the surface allows the SLIS anti-sticking behavior to prevail over adhesive property of the PDMS substrate. When performing 15 min exposure and additional 2 min with sputtered water, the hysteresis values increase with a factor 2 for the whole surface tension range.

Fig. 7b shows hysteresis as a function of surface tension measured on O_2CF_4-OTS-SO350 samples after 50 and 70 water-dipping cycles. By comparison with **Fig. 7**a hysteresis values are consistent with digital microscopy images (monitoring the lubricant covering rate) whatever the shear-depletion test (wind-blowing or water-dipping). After 2 min at 78m/s with 10 ml sputtered water or after 50 cycles of water-dipping, lubricant covering rate reached about 50 % of the total surface, corresponding to hysteresis values lower than 10°, regardless the surface tension. After 15 min and a further 2 min with sputtered water at 78 m/s or after 70 cycles of water dipping, the lubricant covering rate has dropped to about 40 % and hysteresis values recorded at the lowest surface tension value start rising indicating that SLIS is undergoing slight degradation after prolonged exposure.

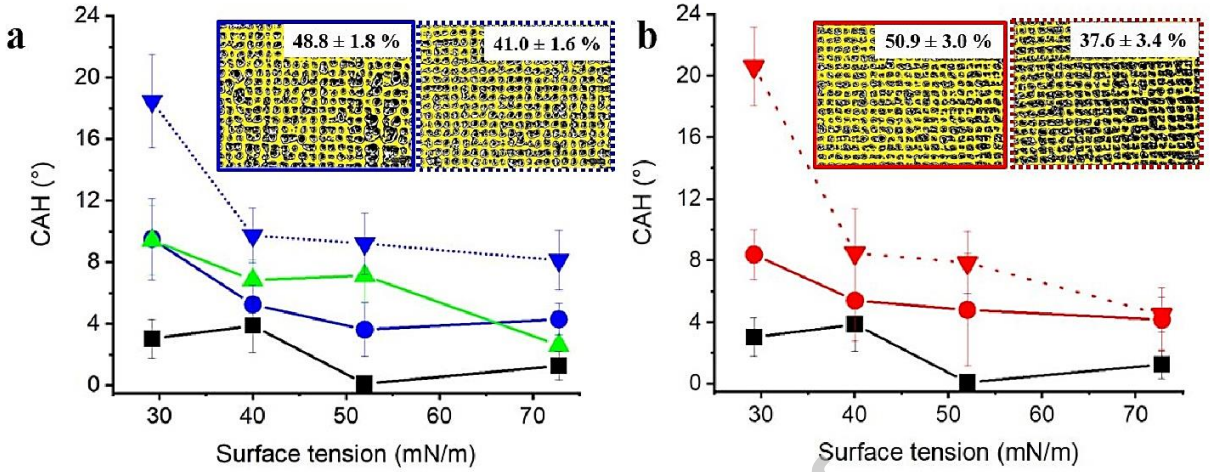

Fig. 7. Contact Angles Hysteresis as a function of surface tension measured on O_2CF_4-OTS-SO350 samples after spin-coating at 2500 rpm (black), (a) after wind tunnel exposure at 78 m/s for 2 min (green) and for 2 min with 10 ml sputtered water (blue), after 0 min (full line) or 15 min of dry exposure (dash line) and (b) after 50 (full line) and 70 (dash line) water-dipping cycles. Inset images are corresponding digital image of lubricant level with the covering rate.

4. Discussion and conclusion

The designed all-polymer SLIS made by a non-hazardous and scalable process offer great potential for glass coating compatible with various kind of applications. Self-peeled PDMS films of 200 µm thick were developed by double replication molding from a laser-ablated mold. We have developed an original texturized surface with micrometric structures offering deep lubricant tank [12,16]. Deep opened-reservoir combined with cross-linked PDMS swelling are undoubtedly the main advantage of SLIS to compete with SLIPS. Combined with cross-linked PDMS abrasive resistance, it allows the lubricant fast replenishment on the surface. We evinced that the amount of infused oil was lower for high viscosity oil even with optimized infusion procedure (low sample thickness, heating, under vacuum). However, high viscosity lubricants have higher shear-resistance. We have also demonstrated by qualitative visualization of lubricant level by digital microscopy and CAH measurements, that introduction of hierarchical structure and adequate chemical functionalization with OTS can delay the appearance of the strongly adhesive PDMS microstructures. These treatments provide a synergy to limit the lubricant loss until hundred successive water-dipping cycles and wind exposure, up to 78 m/s combined with small amount of sputtered water. However, extended wind-blowing exposure and several hundred cycles of water immersion cause severe and irreversible lubricant loss leading to

unavoidable drop pinning and severe loss of transparency due to progressive emerging micro-hills.

Different laser parameters or additional mechanical friction can be used to get rid of the micrometric hills responsible from loss of transparency and drop impalement. It is also possible to maintain transparency and shear-resistance by spin-coating a mixture of PDMS and silicone oil at the final step acting as a protective layer [19].

In this study, original ageing tests combined with lubricant covering rate monitoring and important hysteresis measurements, for a large surface tension range, were used to characterized the oil surfaces stability of cross-linked PDMS based SLIS. This research can be applied in many fields where both transparency and anti-biofouling properties are required [56]. For instance, biofouling in lab-on-chip microfluidic devices made from cross-linked PDMS could have detrimental impact such as cross-contamination between samples to test or led to loss of compounds of interest. A low-friction surface (sliding liquid) facilitates liquid transport and requires less actuating energy (pressure, electrical…). Transparency, when using lab-on-chip device, is notably important when optical read-out is used for biosensing for instance. In addition, those fluorine-free SLIS based elastomer, can be easily transferable on glass (ex. roll-to-roll method) which is also a great assets for camera objectives or optical fiber coatings from medical purposes to out-door use under harsh conditions (marine biofouling, icephobic surfaces to name a few). Finally, such anti-fouling and transparent elastomer could be used as medical devices properties by themselves such as intraocular or contact lenses, medical tubing (ex. catheters…) Naturally, such SLIS are good candidates for high-speed transport as they exhibit good abrasive-resistance and shear-resistance under hard wind and water exposure.

Associated content

Supporting information

Additional figures (PDF):

Scheme of the wind-blowing chamber

SEM top and/or side view images of stainless steel mold, and negatives and positive PDMS replicates

Table of roughness parameters assessed from digital microscopy images

Comparison of PFTS and CHF_3 coating for PFPE-lubricant infusion

EDX spectra on O_2CF_4 etch surfaces and hysteresis angles of the SO350 infused sample after spin-coating at 2500 rpm

Comparison of hysteresis angles and sliding angles measured on SO infused samples and K522 samples after spin-coating, and 30 and 50 water-dipping cycles

Comparison of OTS-SO350 (blue) and CHF_3-K522 hysteresis after water dipping up to 50 cycles

Comparison of hysteresis angles measured on chemically (OTS) and topographically (O_2CF_4 etching) modified samples after different numbers of water-dipping cycles

Silicone oil covering rate as a function of the number of water immersion cycles

Contact angles as function of the surface tensions measured on SO infused samples (after wind-blowing or water dipping tests)

Video File (MP4):

Lubricant self-replenishment observed on O_2CF_4-OTS-SO350 sample after 70 cycles of water dipping and surface scratching with a tweezer

Acknowledgements

The authors acknowledge support from the Région Hauts-de-France, StartAIRR project 'SAATHAF' and the French National Agency (ANR) for its financial supports (ECONOMICS 1340 Project ANR-17-CE08-0032). This work was supported by the French government through the National Research Agency (ANR) under program PIA EQUIPEX LEAF ANR-11-EQPX-0025. This research work has been partially undertaken with the support of IEMN fabrication (CMNF) and was partially supported by the French RENATECH network.

Reference

[1] S. Zouaghi, T. Six, S. Bellayer, S. Moradi, S.G. Hatzikiriakos, T. Dargent, V. Thomy, Y. Coffinier, C. André, G. Delaplace, M. Jimenez, Antifouling Biomimetic Liquid-Infused Stainless Steel: Application to Dairy Industrial Processing, ACS Appl. Mater. Interfaces. 9 (2017) 26565–26573. https://doi.org/10.1021/acsami.7b06709.

[2] T. Karkantonis, A. Gaddam, T. Long, S.S. Joshi, S. Dimov, Femtosecond laser-induced

sub-micron and multi-scale topographies for durable lubricant impregnated surfaces for food packaging applications, Surf. Coat. Technol. 399 (2020) 126166. https://doi.org/10.1016/j.surfcoat.2020.126166.

[3] Q. Liu, Y. Yang, M. Huang, Y. Zhou, Y. Liu, X. Liang, Durability of a lubricant-infused Electrospray Silicon Rubber surface as an anti-icing coating, Appl. Surf. Sci. 346 (2015) 68–76. https://doi.org/10.1016/j.apsusc.2015.02.051.

[4] S. Sunny, G. Cheng, D. Daniel, P. Lo, S. Ochoa, C. Howell, N. Vogel, A. Majid, J. Aizenberg, Transparent antifouling material for improved operative field visibility in endoscopy, Proc. Natl. Acad. Sci. U. S. A. 113 (2016) 11676–11681. https://doi.org/10.1073/pnas.1605272113.

[5] C.S. Ware, T. Smith-palmer, S. Peppou-chapman, L.R.J. Scarratt, E.M. Humphries, D. Balzer, C. Neto, Marine Antifouling Behavior of Lubricant-Infused Nanowrinkled Polymeric Surfaces, 10 (2018) 4173−4182. https://doi.org/10.1021/acsami.7b14736.

[6] H. Sun, R. Li, H. Li, Z. Weng, G. Wu, P. Kerns, S. Suib, X. Wang, Y. Zhang, Bioinspired Oil-Infused Slippery Surfaces with Water and Ion Barrier Properties, ACS Appl. Mater. Interfaces. 13 (2021) 33464–33476. https://doi.org/10.1021/acsami.1c06632.

[7] R. Dufour, M. Harnois, Y. Coffinier, V. Thomy, R. Boukherroub, V. Senez, Engineering Sticky Superomniphobic Surfaces on Transparent and Flexible PDMS Substrate, Langmuir. 26 (2010) 17242–17247.

[8] A.O. Ijaola, E.A. Bamidele, C.J. Akisin, I.T. Bello, A.T. Oyatobo, A. Abdulkareem, P.K. Farayibi, E. Asmatulu, Wettability Transition for Laser Textured Surfaces: A Comprehensive Review, Surfaces and Interfaces. 21 (2020) 100802. https://doi.org/10.1016/j.surfin.2020.100802.

[9] S.M. Varughese, N. Bhandaru, Durability of submerged hydrophobic surfaces, Soft Matter. 16 (2020) 1692–1701. https://doi.org/10.1039/c9sm01942a.

[10] T.S. Wong, S.H. Kang, S.K.Y. Tang, E.J. Smythe, B.D. Hatton, A. Grinthal, J. Aizenberg, Bioinspired self-repairing slippery surfaces with pressure-stable omniphobicity, Nature. 477 (2011) 443–447. https://doi.org/10.1038/nature10447.

[11] S. Peppou-chapman, C. Neto, J.K. Hong, A. Waterhouse, S. Peppou-chapman, Life and death of liquid-infused surfaces: a review on the choice, analysis and fate of the infused liquid layer, Chem. Soc. Rev. 49 (2020) 3688–3715. https://doi.org/10.1039/D0CS00036A.

[12] K. Doll, E. Fadeeva, J. Schaeske, T. Ehmke, A. Winkel, A. Heisterkamp, B.N. Chichkov, M. Stiesch, N.S. Stumpp, Development of Laser-Structured Liquid-Infused Titanium with Strong Biofilm-Repellent Properties, 9 (2017) 9359−9368. https://doi.org/10.1021/acsami.6b16159.

[13] S.J. Goodband, S. Armstrong, H. Kusumaatmaja, K. Voïtchovsky, Effect of Ageing on the Structure and Properties of Model Liquid-Infused Surfaces, Langmuir. 36 (2020) 3461–3470. https://doi.org/10.1021/acs.langmuir.0c00059.

[14] F. Yeganehdoust, A. Amer, N. Shari, I. Karimfazli, A. Dolatabadi, Droplet Mobility on Slippery Lubricant Impregnated and Superhydrophobic Surfaces under the Effect of Air Shear Flow, (2021). https://doi.org/10.1021/acs.langmuir.1c00726.

[15] N. Bjelobrk, H.L. Girard, S.B. Subramanyam, H.M. Kwon, D. Quéré, K.K. Varanasi, Thermocapillary motion on lubricant-impregnated surfaces, Phys. Rev. Fluids. 1 (2016) 1–7. https://doi.org/10.1103/PhysRevFluids.1.063902.

[16] Philseok Kim, Michael J. Kreder, Jack Alvarenga, J. Aizenberg, Hierarchical or Not? Effect of the Length Scale and Hierarchy of the Surface Roughness on Omniphobicity of Lubricant-Infused Substrates, NanoLett. (2021).

[17] E. Afonso, A. Martínez-Gómez, P. Tiemblo, N. García, Industrially viable method for producing all-polymer hydrophobic surfaces apt for slippery liquid-infused substrates, Appl. Surf. Sci. 535 (2021) 147728. https://doi.org/10.1016/j.apsusc.2020.147728.

[18] X. Wang, C. Xiao, H. Liu, Q. Huang, J. Hao, H. Fu, Poly(vinylidene fluoride-hexafluoropropylene) porous membrane with controllable structure and applications in efficient oil/water separation, Materials (Basel). 11 (2018). https://doi.org/10.3390/ma11030443.

[19] W. Cui, T.A. Pakkanen, Fabrication of transparent icephobic surfaces with self-reparability: Effect of structuring and thickness of the lubricant-elastomer layer, Appl. Surf. Sci. 504 (2020) 144061. https://doi.org/10.1016/j.apsusc.2019.144061.

[20] P.S. Kazaryan, M.A. Agalakova, E.P. Kharitonova, M.O. Gallyamov, M.S. Kondratenko, Reducing the contact angle hysteresis of thin polymer films by oil impregnation in supercritical carbon dioxide, Prog. Org. Coatings. 154 (2021). https://doi.org/10.1016/j.porgcoat.2021.106202.

[21] S. Baek, K. Yong, Impact dynamics on SLIPS: Effects of liquid droplet's surface tension and viscosity, Appl. Surf. Sci. 506 (2020). https://doi.org/10.1016/j.apsusc.2019.144689.

[22] F.H. Rajab, Z. Liu, T. Wang, L. Li, Controlling bacteria retention on polymer via replication of laser micro/nano textured metal mould, Opt. Laser Technol. 111 (2019) 530–536. https://doi.org/10.1016/j.optlastec.2018.10.031.

[23] X. Wang, H. Zheng, Y. Wan, W. Feng, Y.C. Lam, Picosecond Laser Surface Texturing of a Stavax Steel Substrate for Wettability Control, Engineering. 4 (2018) 816–821. https://doi.org/10.1016/j.eng.2018.10.006.

[24] S. Bandyopadhyay, S.M. Sriram, V. Parihar, S. Das Gupta, R. Mukherjee, S. Chakraborty, Tunable adhesion and slip on a bio-mimetic sticky soft surface, Soft Matter. 15 (2019) 9031–9040. https://doi.org/10.1039/c9sm01680e.

[25] J.D. Smith, R. Dhiman, S. Anand, E. Reza-Garduno, R.E. Cohen, G.H. McKinley, K.K. Varanasi, Droplet mobility on lubricant-impregnated surfaces, Soft Matter. 9 (2013) 1772–1780. https://doi.org/10.1039/c2sm27032c.

[26] U. Lang, P. Rust, J. Dual, Towards fully polymeric MEMS: Fabrication and testing of PEDOT/PSS strain gauges, Microelectron. Eng. 85 (2008) 1050–1053. https://doi.org/10.1016/j.mee.2008.01.051.

[27] S. Bandyopadhyay, S. Khare, N. Bhandaru, R. Mukherjee, S. Chakraborty, High Temperature Durability of Oleoplaned Slippery Copper Surfaces, Langmuir. 36 (2020) 4135–4143. https://doi.org/10.1021/acs.langmuir.9b03940.

[28] D. Gong, J. Long, D. Jiang, P. Fan, H. Zhang, L. Li, M. Zhong, Robust and Stable Transparent Superhydrophobic Polydimethylsiloxane Films by Duplicating via a

Femtosecond Laser-Ablated Template, ACS Appl. Mater. Interfaces. 8 (2016) 17511–17518. https://doi.org/10.1021/acsami.6b03424.

[29] N. Bhandaru, N. Agrawal, M. Banik, R. Mukherjee, A. Sharma, Hydrophobic recovery of cross-linked polydimethylsiloxane films and its consequence in soft nano patterning, Bull. Mater. Sci. 43 (2020). https://doi.org/10.1007/s12034-020-02162-y.

[30] U.U. Ghosh, S. Nair, A. Das, R. Mukherjee, S. Dasgupta, Replicating and resolving wetting and adhesion characteristics of a Rose petal, Colloids Surfaces A. 561 (2019) 9–17. https://doi.org/10.1016/j.colsurfa.2018.10.028.

[31] M.M. Stanton, R.E. Ducker, J.C. MacDonald, C.R. Lambert, W. Grant McGimpsey, Super-hydrophobic, highly adhesive, polydimethylsiloxane (PDMS) surfaces, J. Colloid Interface Sci. 367 (2012) 502–508. https://doi.org/10.1016/j.jcis.2011.07.053.

[32] A. Ansari, R. Trehan, C. Watson, S. Senyo, Increasing silicone mold longevity: a review of surface modification techniques for PDMS-PDMS double casting, Soft Mater. 19 (2021) 388–399. https://doi.org/10.1080/1539445X.2020.1850476.

[33] I. Sotiri, A. Tajik, Y. Lai, C.T. Zhang, Y. Kovalenko, C.R. Nemr, H. Ledoux, E. Johnson, H.S. Patanwala, J.V.I. Timonen, Y. Hu, J. Aizenberg, Tunability of liquid-infused silicone materials for biointerfaces, Biointerphases. 13 (2018) 06D401. https://doi.org/10.1116/1.5039514.

[34] C. Howell, T.L. Vu, C.P. Johnson, X. Hou, O. Ahanotu, J. Alvarenga, D.C. Leslie, O. Uzun, A. Waterhouse, P. Kim, M. Super, M. Aizenberg, D.E. Ingber, J. Aizenberg, Stability of surface-immobilized lubricant interfaces under flow, Chem. Mater. 27 (2015) 1792–1800. https://doi.org/10.1021/cm504652g.

[35] C. Liu, Y. Li, C. Lu, Y. Liu, S. Feng, Y. Liu, Robust Slippery Liquid-Infused Porous Network Surfaces for Enhanced Anti-icing / Deicing Performance, ACS Appl. Mater. Interfaces. 12 (2020) 25471–25477.

[36] N. Vogel, R.A. Belisle, B. Hatton, T. Wong, J. Aizenberg, Transparency and damage tolerance of patternable omniphobic lubricated surfaces based on inverse colloidal monolayers, Nat. Commun. (2013). https://doi.org/10.1038/ncomms3176.

[37] S. Barthwal, B. Lee, S. Lim, Applied Surface Science Fabrication of robust and durable slippery anti-icing coating on textured superhydrophobic aluminum surfaces with infused silicone oil, Appl. Surf. Sci. 496 (2019) 143677. https://doi.org/10.1016/j.apsusc.2019.143677.

[38] A. Jain, A.D. van der Meer, A.L. Papa, R. Barrile, A. Lai, B.L. Schlechter, M.A. Otieno, C.S. Louden, G.A. Hamilton, A.D. Michelson, A.L. Frelinger, D.E. Ingber, Assessment of whole blood thrombosis in a microfluidic device lined by fixed human endothelium, Biomed. Microdevices. 18 (2016) 1–7. https://doi.org/10.1007/s10544-016-0095-6.

[39] M.E. Vlachopoulou, A. Tserepi, P. Pavli, P. Argitis, M. Sanopoulou, K. Misiakos, A low temperature surface modification assisted method for bonding plastic substrates, J. Micromechanics Microengineering. 19 (2009). https://doi.org/10.1088/0960-1317/19/1/015007.

[40] R. Dufour, G. Perry, M. Harnois, Y. Coffinier, V. Thomy, V. Senez, From micro to nano reentrant structures : hysteresis on superomniphobic surfaces, (2013) 409–415.

https://doi.org/10.1007/s00396-012-2750-7.

[41] S. Sett, X. Yan, G. Barac, L.W. Bolton, N. Miljkovic, Lubricant-Infused Surfaces for Low-Surface-Tension Fluids: Promise versus Reality, ACS Appl. Mater. Interfaces. 9 (2017) 36400–36408. https://doi.org/10.1021/acsami.7b10756.

[42] X. Chen, G. Wen, Z. Guo, What are the design principles, from the choice of lubricants and structures to the preparation method, for a stable slippery lubricant-infused porous surface?, Mater. Horizons. 7 (2020) 1697–1726. https://doi.org/10.1039/d0mh00088d.

[43] G. Perry, Y. Coffinier, V. Thomy, R. Boukherroub, Sliding droplets on superomniphobic zinc oxide nanostructures, Langmuir. 28 (2012) 389–395. https://doi.org/10.1021/la2035032.

[44] P. Hu, Q. Xie, G. Zhang, Silicone-Based Fouling-Release Coatings for Marine Antifouling, (2020). https://doi.org/10.1021/acs.langmuir.9b03926.

[45] S. Basu, B.M. Hanh, J.Q. Isaiah Chua, D. Daniel, M.H. Ismail, M. Marchioro, S. Amini, S.A. Rice, A. Miserez, Green biolubricant infused slippery surfaces to combat marine biofouling, J. Colloid Interface Sci. 568 (2020) 185–197. https://doi.org/10.1016/j.jcis.2020.02.049.

[46] G. McHale, N. Afify, S. Armstrong, G.G. Wells, R. Ledesma-Aguilar, The Liquid Young's Law on SLIPS: Liquid-Liquid Interfacial Tensions and Zisman Plots, Langmuir. 38 (2022) 10032–10042. https://doi.org/10.1021/acs.langmuir.2c01470.

[47] G. Boveri, A. Corozzi, F. Veronesi, M. Raimondo, Different approaches to low-wettable materials for freezing environments: Design, performance and durability, Coatings. 11 (2021) 1–16. https://doi.org/10.3390/coatings11010077.

[48] S. Sahoo, R. Mukherjee, Evaporative drying of a water droplet on liquid infused sticky surfaces, Colloids Surfaces A Physicochem. Eng. Asp. 657 (2023) 130514. https://doi.org/10.1016/j.colsurfa.2022.130514.

[49] C. Semprebon, G. McHale, H. Kusumaatmaja, Apparent contact angle and contact angle hysteresis on liquid infused surfaces, Soft Matter. 13 (2017) 101–110. https://doi.org/10.1039/C6SM00920D.

[50] J. Garra, T. Long, J. Currie, T. Schneider, R. White, M. Paranjape, Dry etching of polydimethylsiloxane for microfluidic systems, J. Vac. Sci. Technol. A Vacuum, Surfaces, Film. 20 (2002) 975–982. https://doi.org/10.1116/1.1460896.

[51] D. Ebert, B. Bhushan, Transparent, superhydrophobic, and wear-resistant surfaces using deep reactive ion etching on PDMS substrates, J. Colloid Interface Sci. 481 (2016) 82–90. https://doi.org/10.1016/j.jcis.2016.07.035.

[52] T.-P. Dominique, Sohounhloue; Louis, Tenebre; Mireille, Privat; Jean-Marc, Douillard; René, Bennes; Emmanuel, Thermodynamic properties and structure of the water-ethanol silicone oil interface, Can. J. Chem. (1986) 2299.

[53] S. Peppou-chapman, C. Neto, Mapping Depletion of Lubricant Films on Antibiofouling Wrinkled Slippery Surfaces, (2018). https://doi.org/10.1021/acsami.8b11768.

[54] C. Liu, Y. Li, C. Lu, Y. Liu, S. Feng, Y. Liu, Robust Slippery Liquid-Infused Porous Network Surfaces for Enhanced Anti-icing / Deicing Performance, (2020) 0–6.

[55] J. Yong, F. Chen, Q. Yang, Y. Fang, J. Huo, J. Zhang, X. Hou, Nepenthes Inspired Design of Self-Repairing Omniphobic Slippery Liquid Infused Porous Surface (SLIPS) by Femtosecond Laser Direct Writing, Adv. Mater. Interfaces. 4 (2017) 1–7. https://doi.org/10.1002/admi.201700552.

[56] M. Villegas, Z. Cetinic, A. Shakeri, T.F. Didar, Fabricating smooth PDMS microfluidic channels from low-resolution 3D printed molds using an omniphobic lubricant-infused coating, Anal. Chim. Acta. 1000 (2018) 248–255. https://doi.org/10.1016/j.aca.2017.11.063.

TOC

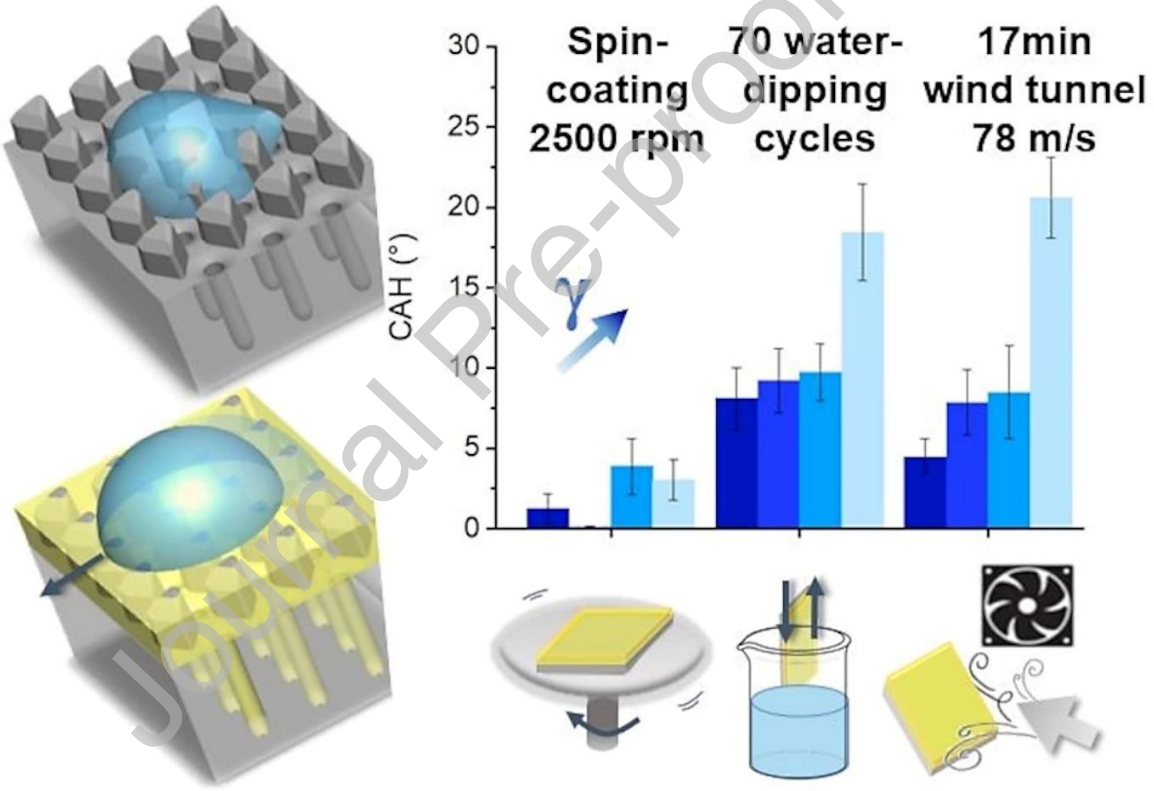

Declaration of interests

☐ The authors declare that they have no known competing financial interests or personal relationships that could have appeared to influence the work reported in this paper.

☒ The authors declare the following financial interests/personal relationships which may be considered as potential competing interests:

Vincent Thomy reports financial support was provided by SATT Network. Yannick Coffinier reports financial support was provided by French National Research Agency.